# FURTHER RESULTS ON $\pi^- p \rightarrow K^o Y^o$ IN THE FORWARD DIRECTION AT 6, 8 AND 11.2 GEV/C.

E. BERTOLUCCI, I. MANNELLI, G. PIERAZZINI, A. SCRIBANO, F. SERGIAMPIETRI, M.L. VINCELLI - Istituto di Fisica dell' Università di Pisa and I.N.F.N., Sezione di Pisa, Italy

and

C. CAVERZASIO, J.P. GUILLAUD[+], L. HOLLOWAY, M. YVERT - Institut du Radium, Orsay, France

## ABSTRACT

A spark chamber experiment to measure the $\pi^- p \rightarrow K^o Y^o$ associated production at high energy has been recently completed at the CERN PS. Data has been taken at 6,8,10, 11.2 GeV/c for the incident $\pi^-$ momentum. We present here further results (Ref.1) at 6, 8 and 11.2 GeV/c based on ~1100, 1300 and 3000 events (about 60%, 65% and 90% of the available statistics) respectively selected for the differential cross sections.

The sum of the $\pi^- p \rightarrow K^o \Lambda^o$ and $\pi^- p \rightarrow K^o \Sigma^o$ differential cross sections is strongly peaked in the forward direction and can be well fitted, for $|t_{min}| \leq |t| \leq 0.4$ $(GeV/c)^2$, by an exponential shape $e^{at}$ with $a=8.0\pm0.5$ at 6, $a=7.7\pm0.5$ at 8 and $a=7.8\pm0.4$ $(GeV/c)^{-2}$ at 11.2 GeV/c. The integral over the interval $|t_{min}| \leq |t| \leq 1.01$ $(GeV/c)^2$ gives $40.5\pm6$ μb at 6, $25.3\pm4$ μb at 8 and $18\pm3$ μb at 11.2 GeV/c, including systematic errors.

A comparison is made with previous bubble and spark chamber results and Regge Poles fits.

---

[+] CERN Fellow.

## 1.- EXPERIMENTAL APPARATUS.

The experimental apparatus is shown schematically in Fig.1. The $\pi^-$ beam, tipically $10^5$ particles per burst, is focused on the 1.5 cm diameter, 10 cm long liquid hydrogen target(1), which is concentric with a cylindrical spark chamber containing both thin Al and Pb plates. The beam is defined electronically by four scintillation and two Cerenkov counters. Two hodoscopes, with 7×2 and 7×7 elements respectively, determine the incident $\pi^-$ position with a ±.2 cm uncertainty at the target and ±.5 cm at the last spark chamber.

A picture is taken each time an incident $\pi^-$ fails to give a pulse in the anticoincidence counter surrounding the target while at the same time a pulse is detected in the counter placed in front of the second spark chamber.

The hodoscope information is then BCD coded and displayed on the same film where the 90° stereo images(2) of the spark chambers are recorded. While the two thin Al foil S.C. are designed to detect the charged tracks with a minimum of multiple scattering, the last spark chamber(about 15 rad.lenghts of Pb) allows also the detection of forward emitted $\gamma$-rays. We have found that in about 1 out of 10 pictures a single V type event is present, while in the majority of the others there is at least one $\gamma$-ray.

## 2.- ANALYSIS AND SELECTION OF EVENTS.

The V type events selected by the scanners are measured on digitized tables. The coordinates of the sparks are reconstructed in true space with an accuracy of ±.06 cm. A plane is fitted through them and straight lines are fitted through the sparks which belong to the same track. The intersection of the best fit plane with the incident $\pi^-$, as defined by the two hodoscopes, is taken as the interaction point; the intersection of the two best fit lines as the neutral strange particle decay vertex. The line joining the interac-

tion with the decay vertex is assumed to coincide with the direction of emission of the strange particle. We then calculate the partial angle $\bar{\theta}$, formed by this direction and the nearest of the two charged prongs, and the total angle $\theta$ between them. On the assumption that the observed event is indeed a $K^0_S \to \pi^+\pi^-$ decay, the K° momentum is evaluated (Fig.2) together with the invariant mass of the associated recoil and the other kinematical quantities of interest.

Events are selected on the basis of coplanarity, collinearity, opening angle, recoil mass, position of decay and interactions points.

The effect of the cuts introduced by the acceptance criteria have been extensively studied by comparing the experimental distributions with the Montecarlo simulated ones for various hypothesis about the production processes. We have been able to fit satisfactorily every significant experimental distribution and this gives us confidence on the calculated efficiencies.

Fig.3a shows the reconstructed recoil mass distribution at 6 GeV/c for events, within the fiducial volume, which satisfy the coplanarity and collinearity requirements.

In Fig.3b the analogus, Montecarlo generated distributions for $\Lambda^\circ+\Sigma^\circ$, $Y^*(1385)$ and $Y^*(1519)$ are shown, normalized to the values which produce the best fit linear combination to the experimental data (dotted line in Fig.3a). It is possible to make a cut which selects events, produced in association with a $\Lambda^\circ$ or $\Sigma^\circ$ recoil, with about equal efficiencies, while only a small fraction of the events with an isobar as recoil enter in the cut.

The resolution in recoil mass, while it is independent of the momentum transfer and mass values, is however

a function of the incident momentum and of the spark chambers arrangement. For our running conditions we estimate half widths at half heights of 90, 140 and 200 MeV respectively at 6, 8, and 11.2 GeV/c. This fact, coupled with the rather copious production of all neutral final state isobars in our energy range, has made necessary a detailed study of the accuracy of the 'elastic' selection criteria and of the effects of contamination from isobar events on differential cross sections.

At each energy we have evaluated the contamination within various cuts in recoil mass and opening angle, by fitting the experimental mass distribution with a series of isobars contributions, as briefly mentioned above[3]. We have then subtracted from the momentum transfer distribution of the accepted events the weighted experimental $|t|$ distribution of the events in the recoil mass region from which the contamination is produced.

For each case the differential cross section (see ch.3) has been deduced and by comparing the shapes and absolute values obtained at the same incident momentum for different cuts we have reached the conclusion that the uncertainty due to the method of analysis is smaller than the statistical one.

The empty target contribution (typically 9% of the full target rate) has been subtracted bin by bin from the various distributions.

Fig.4 shows the resolution in the momentum transfer t for various t values at 6 and 11.2 GeV/c.

## 3.- NORMALIZATION.

The incoming flux has been monitored throughout the experiment. Contamination from $e^-$ (0.4-0.2)% and $\mu^-$(2-

1)% has been measured and subtracted at the different energies. Corrections have been made for δ-rays ((4±1)%. A δ-ray produced by the incoming particle before the occurrence of a $\pi^- p \to K^\circ Y^\circ$ interaction can reach the anticoincidence counter and veto the event), strong interactions of the incoming and outgoing particles (about 2.5%), scanning (98%) and measuring (about 95%) efficiencies. For the ratio $K^\circ_S \to \pi^+\pi^-/K^\circ$ we have used the value 0.33.

The effects connected with the lifetime (for which we used the Rosenfeld values) of the $\Lambda^\circ$ (supposed to decay as $\pi^- p$ in 67% of the cases) and $K^\circ_S$ have been incorporated in the Montecarlo program, which also take into account multiple scattering, measuring errors and the limitation of the fiducial volume.

The overall systematic uncertainty has been estimated to be ± 15%.

## 4.- RESULTS.

In Tab.I we list the results for differential and integrated cross sections. In Fig.5, where the differential cross sections are shown, we have also indicated the Montecarlo calculated relative detection efficiency as a function of t. Its variation (essentially independent of the incident momentum) is caused by the changing fraction of $\Lambda \to \pi^- p$ decays which, with a probability depending on the Λ production angle and momentum, trigger the anticoincidence. The values plotted are corrected for it and the errors indicated are statistical only (they include the statistical error for empty target and contamination subtraction).

For $|t|$ smaller than 0.40 $(GeV/c)^2$ the differential cross section can be well fitted by an exponential $e^{at}$ with $a=8.0\pm0.5$ ($\chi^2=14$) at 6, $a=7.7\pm0.5$ ($\chi^2=6$) at 8 and $a=7.8\pm0.4$ $(GeV/c)^{-2}$ ($\chi^2=6$) at 11.2 GeV/c.

Crennel et al.(Ref.2) in a bubble chamber experiment at 6 GeV/c with 448 events obtained the value $a=7.8\pm.5$ $(GeV/c)^{-2}$ and a $\pi^-p \to K^\circ Y^\circ$ total cross section of $41\pm4$ μb.

Ehrlich et al.(Ref.3) with 101 events at 7.91 GeV/c obtained $a\simeq9.7$ $(GeV/c)^{-2}$ and a total cross section of about 32 μb. No other statistically significant data exist above this energy.

Recently Hoang et al.(Ref.4) have reported a spark chamber study of $\pi^-p \to K^\circ Y^\circ$ in the forward and backward direction at 4 GeV/c. They find $a=8.57\pm.38$ $(GeV/c)^{-2}$ for $|t|$ less than 0.4 $(GeV/c)^2$.

A systematic bubble chamber study of two body strange particles production from $\pi^-$ between 1.9 and 4.2 GeV/c is reported by Dahl et al.(Ref.5). Some of the features found at our energies, as the magnitude of the slope and the change of slope at about $|t|\simeq 0.4$ $(GeV/c)^2$ are already present in this range of energy.

We have calculated the total cross section by integrating between $|t| = |t_{min}|$ and $|t|=1.01$ $(GeV/c)^2$. The values obtained are $40.5\pm6$ μb at 6, $25.3\pm4$ μb at 8 and $18\pm3$ μb at 11.2 GeV/c. In Fig.6 they are shown together with previous bubble chamber results. It appears that the trend already present in the 2 to 4 GeV/c region is not in contrast with the new results at higher energy. A good fit to the energy dependence can be obtained with the simple power law $E^{-3.6}$ where E is the CM total energy.

Recently a double Regge Pole exchange model, with exact $SU_3$ symmetry, has been proposed by Ph.Salin(Ref.8) and K.V.L.Sarma and D.D.Reeder (Ref.9) and applied in particular to the description of the associated production reactions. It consists in a rather straightforward extension to these strangeness-exchange processes of the model (Ref.10) successfully used for the $\pi^-p$ and $K^-p$ charge-exchange and for the $\pi^-p \to \eta n$ production.

A comparison of our results, with the calculation of the differential cross section based on the parametrization obtained at lower energies by Sarma and Reeder, shows qualitative agreement. A more detailed study of possible fits within this framework is presently being carried on.

## 5.- TEST MEASUREMENT OF $K^-p \to \overline{K}^0 n$.

During most of the running time we have triggered the spark chambers also on neutral final state $K^-$ interactions. During a short period at 8 GeV/c we have taken data only on $K^-$. Using this sample ( 65% of the available statistics at 8 GeV/c) we have applied our method of analysis to $K^-p \to \overline{K}^0 n$ events.

The main difference is the flatness of the efficiency vs. t, since in this case there is not any more the partial suppression of events, which is caused by $\Lambda$ decays within the anticoincidence counter.

We obtain with 169 events an integrated cross section of $80 \pm 16$ μb for $0 \leq |t| \leq 0.9$ $(GeV/c)^2$. This value and the shape of the differential cross section (Fig.7) are in good agreement with the interpolation of the data of Astbury et al.(Ref.11)at 7.1 and 9.5 GeV/c.

## ACKNOWLEDGEMENTS

We would like to acknowledge the hospitality and support of CERN NP Division and the cooperation of the PS staff; the help received from CEN-Saclay; the collaboration of the Saclay group, who worked at the same time on $\pi^-p \to n\overleftarrow{\pi}^0$, and the dedicated help of our technicians and scanners.

Most of the computations have been performed with the IBM 7090 of the CNUCE-Pisa.

This experiment would not have been possible wi-

thout the special target built by Dr.P.Roubeau at Saclay. We like to thank him and also Mr.Derny, Dr.Borghini, Mr. Vermeulen, Mr.Uldry, Mr.Scherrer for the running of the target.

The enthusiastic support of Prof.P.Falk-Vairant and Prof.G.Stoppini throughout the experiment is gratefully acknowledged.

## FOOTNOTES

(1) This special, He cooled, liquid $H_2$ target, designed by P.Roubeau and built at Saclay, has such geometry that it is possible to surround it with a 2.9 cm diameter anticoincidence counter, to place the last beam defi - ning counter at only 2 cm before the liquid $H_2$ and to insert the whole target-counters assembly in the center of the cylindrical spark chamber, without significantly obstructing its view.

(2) No stereo is provided for the cylindrical spark chamber.

(3) For the cuts considered, the contamination ranged between 3 and 12% at 6 GeV/c and between 15 and 30% at 8 and 11.2 GeV/c.

## REFERENCES


1. INFN/AE-67/9 submitted to the Heidelberg Conference (1967).
2. D.J.Crennel, G.R.Kalbfleisch, K.Wu Lai, J.M.Scarr, Th. G.Schumann, I.O.Skillicorn, M.S.Webster - Phys.Rev.Lett. 18,86 (1967).
3. R.Ehrlich, W.Selove, H.Yuta - Phys.Rev. 152,1194 (1966).
4. T.F.Hoang, Y.S.Kim, S.Margulies, T.H.Groves - Phys.Lett. 25B,615 (1967).
5. O.I.Dahl, L.M.Hardy, R.J.Hess, J.Kirz, D.H.Miller, J.A. Schwartz - Phys.Rev. to be published and UCRL 17217.
6. T.P.Wangler, A.R.Erwin, W.D.Walker - Phys.Rev. 137,B414 (1965).
7. J.Bartsch, et al., Aachen, Hanburg, London, Munchen collaboration - Nuovo Cimento 43,A1010 (1966).
8. Ph. Salin - CERN preprint TH.762 (1967)
9. K.V.L.Sarma and D.D.Reeder - University of Winsconsin pre.
10. K.V.L.Sarma and D.D.Reeder - N.C. 51A,169 (1967).
11. P.Astbury, G.Brautti, G.Finocchiaro, A.Michelini, K.Terwilliger, D.Websdale, C.H.West, P.Zanella, W.Beusch, W. Fischer, B.Gobbi, M.Pepin, E.Polgar - Phys.Lett. 23,396 (1966).
    See also: A.Buffington - Ph.D. Thesis, MIT Cambridge
    $K^- p \to \bar{K}^0 n$ at 8 GeV/c (Dec.1966).

TABLE I

| | | 6 GeV/c $\sigma_T$=40.5±6 μb | 8 GeV/c $\sigma_T$=25.3±4 μb | 11.2 GeV/c $\sigma_T$=18±3 μb |
|---|---|---|---|---|
| $\lvert t \rvert$ (GeV/c)$^2$ | $\Delta t$ | $d\sigma/dt$ | $d\sigma/dt$ μb·GeV$^{-2}$·c$^2$ | $d\sigma/dt$ |
| .02 | .02 | 289 ± 36 | 165 ± 22 | 125 ± 15 |
| .04 | " | 274 ± 32 | 150 ± 19 | 99 ± 12 |
| .06 | " | 156 ± 22 | 109 ± 16 | 93 ± 11 |
| .08 | " | 177 ± 24 | 106 ± 15 | 70 ± 9.5 |
| .10 | " | 131 ± 20 | 65 ± 12 | 56 ± 8.5 |
| .12 | " | 131 ± 19 | 84 ± 13 | 44 ± 7.5 |
| .14 | " | 97 ± 17 | 63 ± 11 | 52 ± 7.5 |
| .16 | " | 104 ± 17 | 56 ± 11 | 40 ± 6.5 |
| .18 | " | 64 ± 14 | 44 ± 10 | 40 ± 6 |
| .20 | " | 52 ± 13 | 40.5 ± 9.5 | 27 ± 5.5 |
| .23 | .04 | 57 ± 8.5 | 32.5 ± 6 | 24.8 ± 3.3 |
| .27 | " | 38 ± 7.5 | 20.8 ± 5 | 17 ± 3 |
| .32 | .06 | 18.5 ± 4.5 | 16.3 ± 3.7 | 9.6 ± 1.9 |
| .38 | " | 21.8 ± 4.2 | 12.8 ± 3.1 | 7.5 ± 1.7 |
| .44 | " | 17.6 ± 3.7 | 7.7 ± 2.5 | 4.9 ± 1.5 |
| .50 | " | 15.4 ± 2.7 | 4.5 ± 1.9 | 4.9 ± 1.3 |
| .58 | .10 | 9.1 ± 1.9 | 6.6 ± 1.4 | 2.9 ± 0.6 |
| .68 | " | 5.5 ± 1.5 | 5.8 ± 1.8 | 1.6 ± 0.6 |
| .87 | .28 | 3.5 ± 0.8 | 3.6 ± 0.5 | 1.9 ± 0.3 |

## FIGURE CAPTIONS

Fig. 1 - Experimental apparatus. ≠ ≠ 2,3',3,4 are the beam defining counters; hod 1 and hod 2 the two hodoscopes, which determine the position of the incident $\pi^-$; ≠ 5 is the anticoincidence counter surrounding the $H_2$ liquid target. The cylindrical spark chamber, not so far used for the analysis, is meant to detect γ-rays produced at large angles, as in $\Sigma^\circ$ or $Y^\circ$ decays, in addition to the charged decay products of the Λ. Two threshold gas Cerenkov counters, used for $\pi^-$ and $K^-$ selection, are not shown. SC1 and SC2 are thin Al-foil spark chambers which detect the charged decay of the strange particles, while the Saclay spark chamber detects also the forward γ-rays. ≠6, in front of SC2, is a coincidence counter.
The figure shows also the triggering logic.

Fig. 2 - $K^\circ \to \pi^+\pi^-$ kinematics at high energy. As it can be seen from the figure a measurement of the total angle θ and partial angle $\bar{\theta}$ is sufficient to determine the $K^\circ$ momentum. For about 85% of the available phase space the lines of constant θ and $\bar{\theta}$ are almost perpendicular to each other and, since lines of constant θ are nearly parallel to lines of constant $K^\circ$ momentum, a good precision can be achieved even when θ (as it happens in our experiment) is rather poorly known in respect to θ.

Fig. 3a- Experimental distribution of the reconstructed recoil mass at 6 GeV/c (see text).

Fig. 3b- Montecarlo distribution of the recoil mass for $\Lambda^\circ+\Sigma^\circ$, $Y^*(1385)$, $Y^*(1519)$.

Fig. 4 - Momentum transfer resolution at 6 and 11.2 GeV/c, for various t values.

Fig. 5 - Differential cross section $d\sigma/dt$ for $\pi^-p \to K^\circ Y^\circ$ at 6, 8, 11.2 GeV/c and relative detection efficiency.
The curves superimposed on the experimental points represent the direct prediction, according to a calculation we performed, which follows from the Sarma and Reeder fit (Ref.9) to the associated production at lower energies.

Fig. 6 - Plot of the experimentally available values for $\sigma_{tot}(\pi^-p \to K^\circ Y^\circ)$, at incident $\pi^-$ momenta above 2 GeV/c.

Fig. 7 - Differential cross section $d\sigma/dt$ for $K^-p \to \bar{K}^\circ n$ at 8 GeV/c.

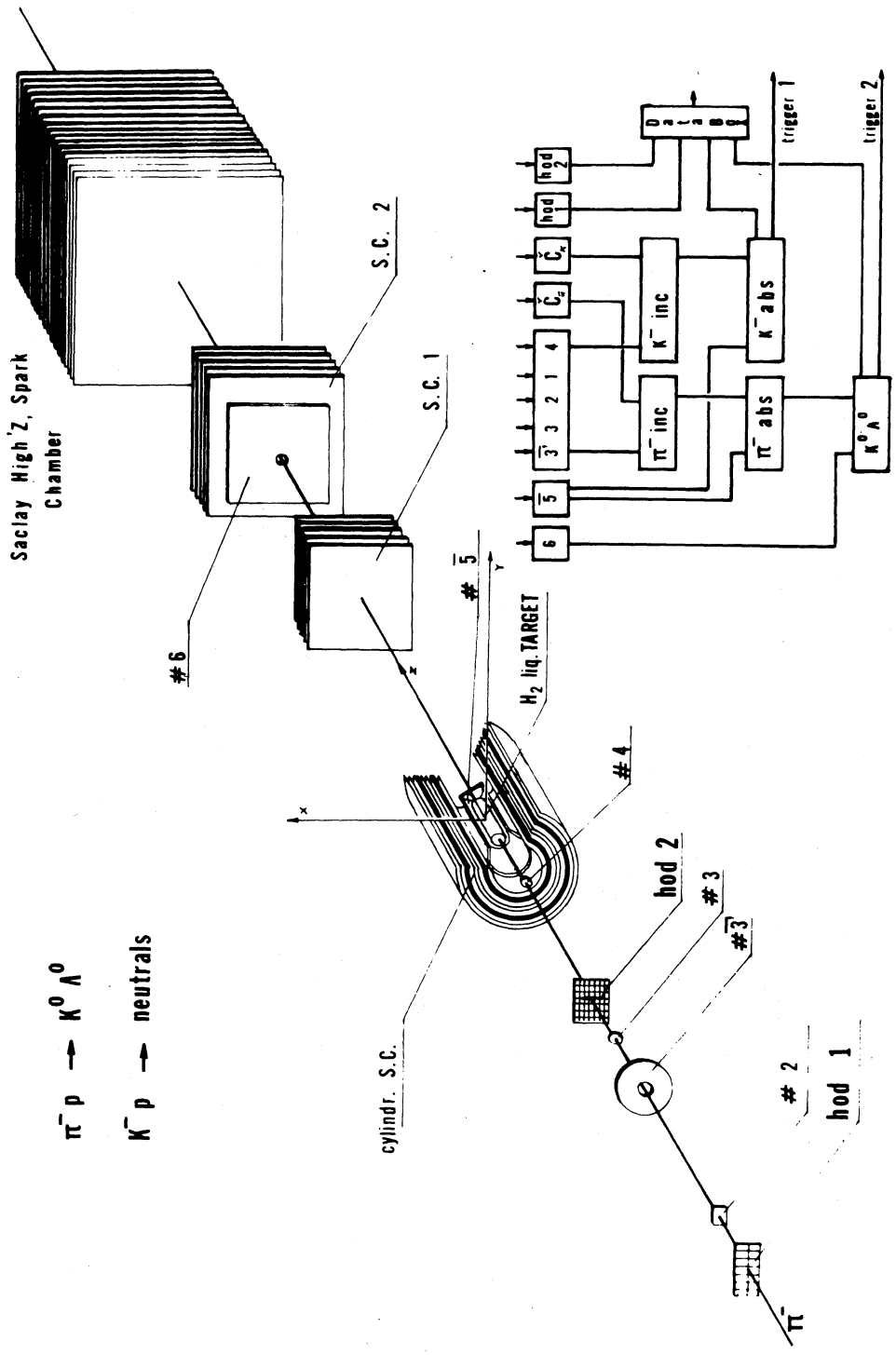
Saclay High'Z, Spark Chamber
S.C. 2
S.C. 1
#6
#5
H2 liq. TARGET
#4
hod 2
#3
#3'
# 2
hod 1
cylindr. S.C.
π⁻
π⁻ p → K⁰ Λ⁰
K⁻ p → neutrals
hod 2
hod 1
K⁻ inc
K⁻ abs
π⁻ inc
π⁻ abs
K⁰ Λ⁰
trigger 1
trigger 2
Data Bus

FIG. 1

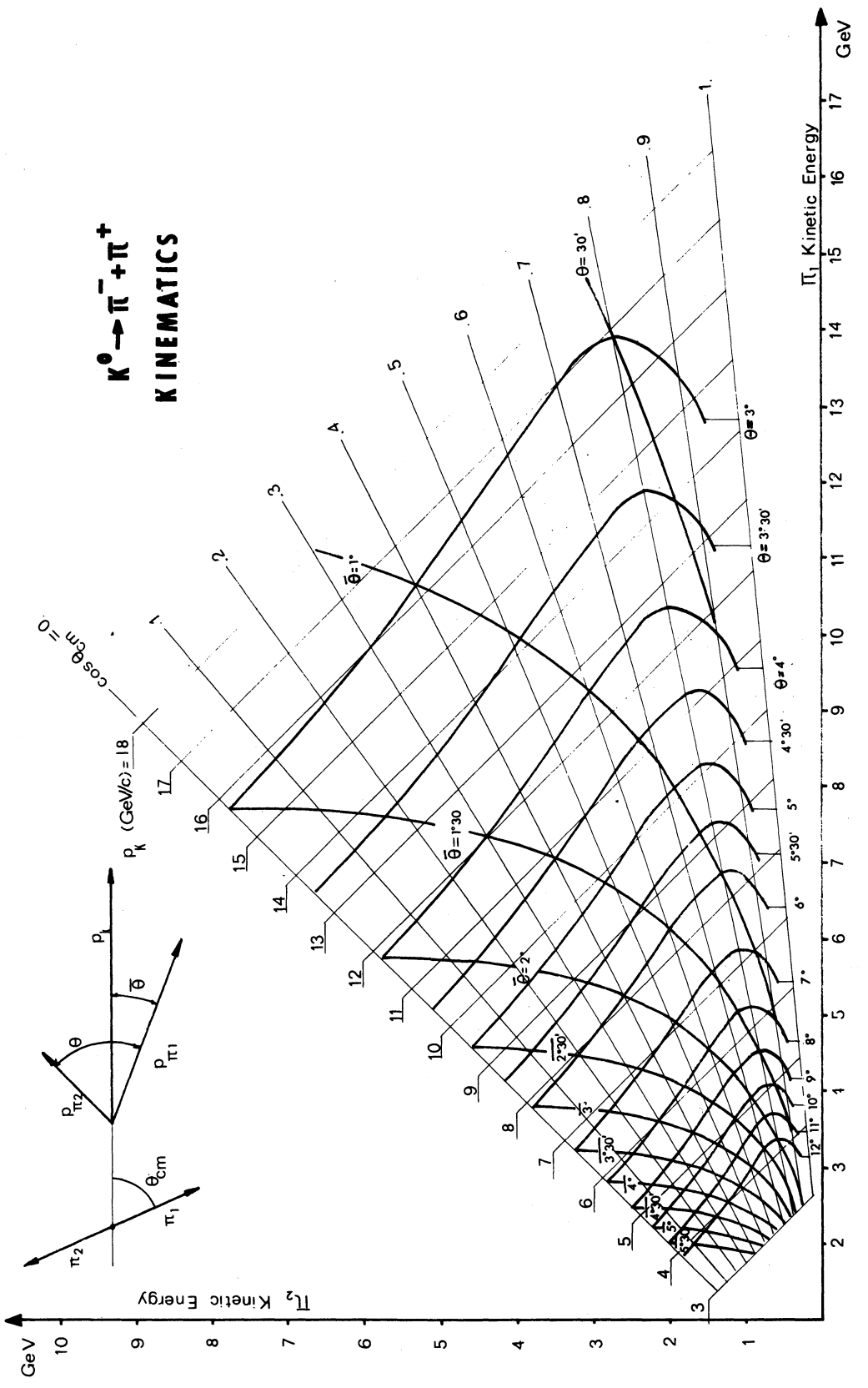
K⁰→π⁻+π⁺
KINEMATICS
Π₂ Kinetic Energy
Π₁ Kinetic Energy
GeV
p_K (GeV/c) = 18
cosθ_cm = 0
θ̄=1°
θ̄=1°30
θ̄=2°
2°30'
3°
3°30'
4°
4°30'
5°
5°30'
6°
7°
8°
9°
10°
11°
12°
θ=30'
θ=3°
θ=3°30'
θ=4°
p_t
θ̄
θ
p_π1
p_π2
θ_cm
π₁
π₂

Fig. 2

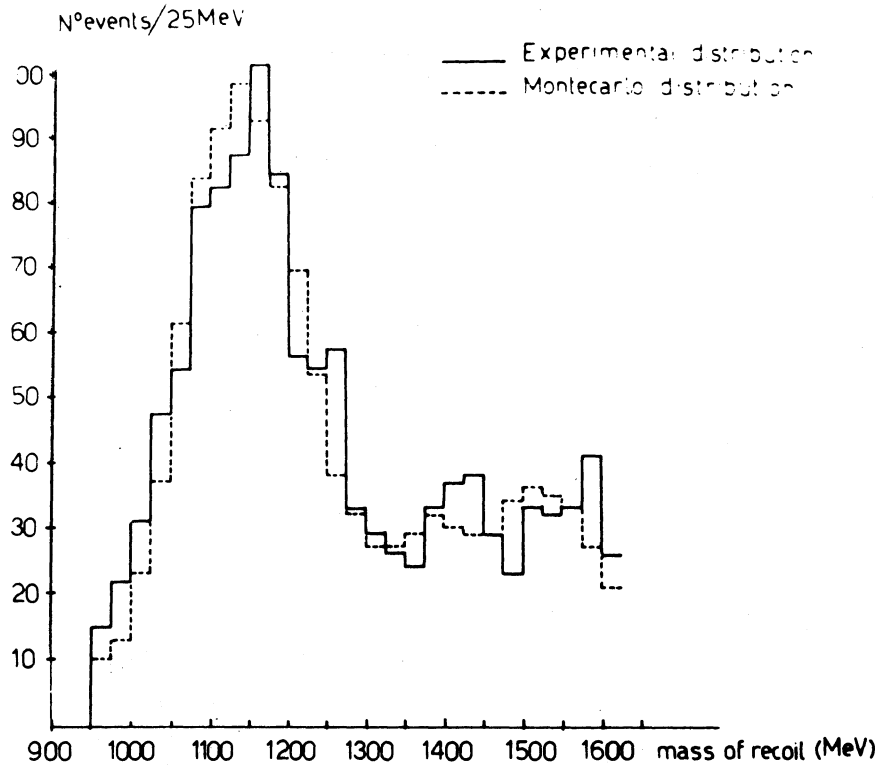
N°events/25MeV
Experimental distribution
Montecarlo distribution
30
90
80
70
60
50
40
30
20
10
900
1000
1100
1200
1300
1400
1500
1600
mass of recoil (MeV)

FIG. 3a

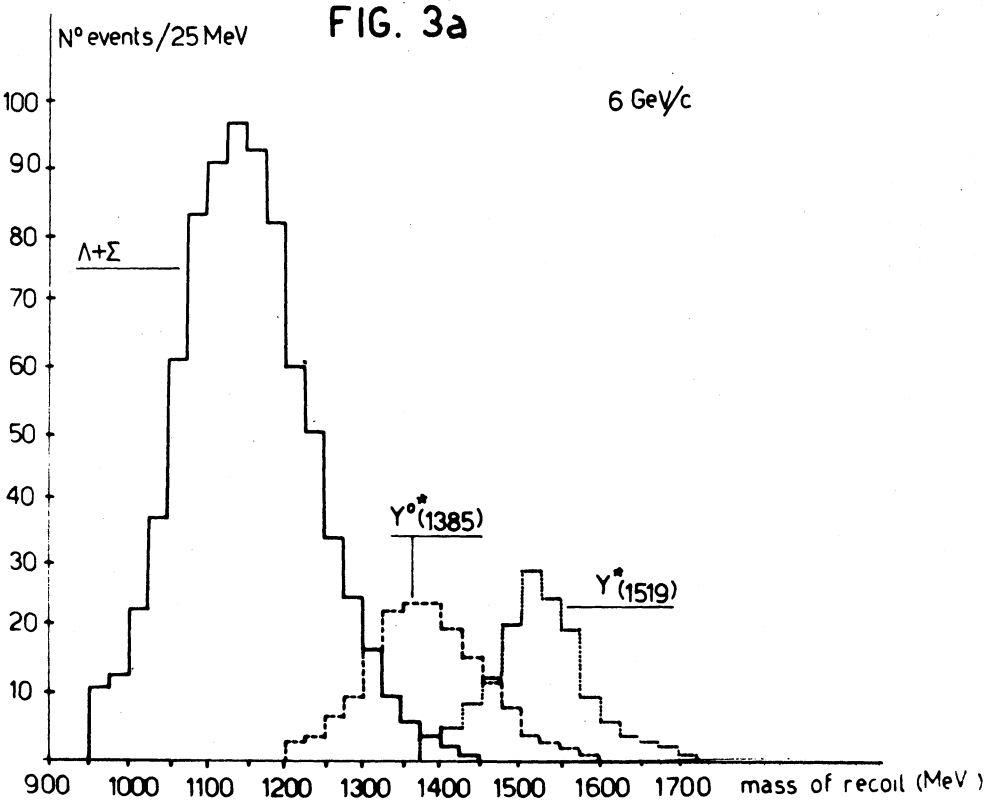
N° events/25 MeV
6 GeV/c
100
90
80
70
60
50
40
30
20
10
Λ+Σ
Y°*(1385)
Y*(1519)
900
1000
1100
1200
1300
1400
1500
1600
1700
mass of recoil (MeV)

FIG. 3b

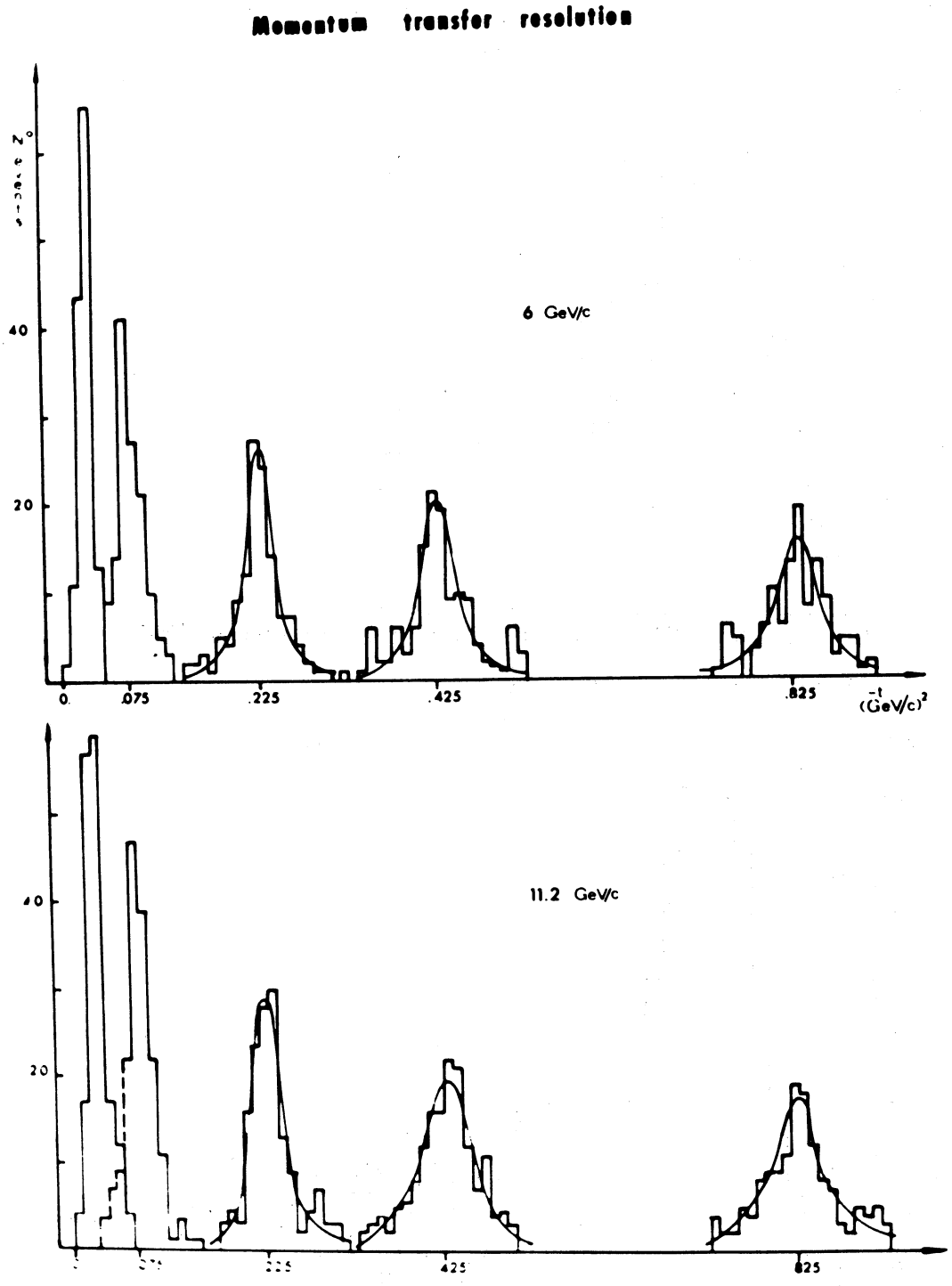
Momentum transfer resolution
6 GeV/c
40
20
0
.075
.225
.425
.825
(GeV/c)²
11.2 GeV/c
40
20
.425
.825

FIG. 4

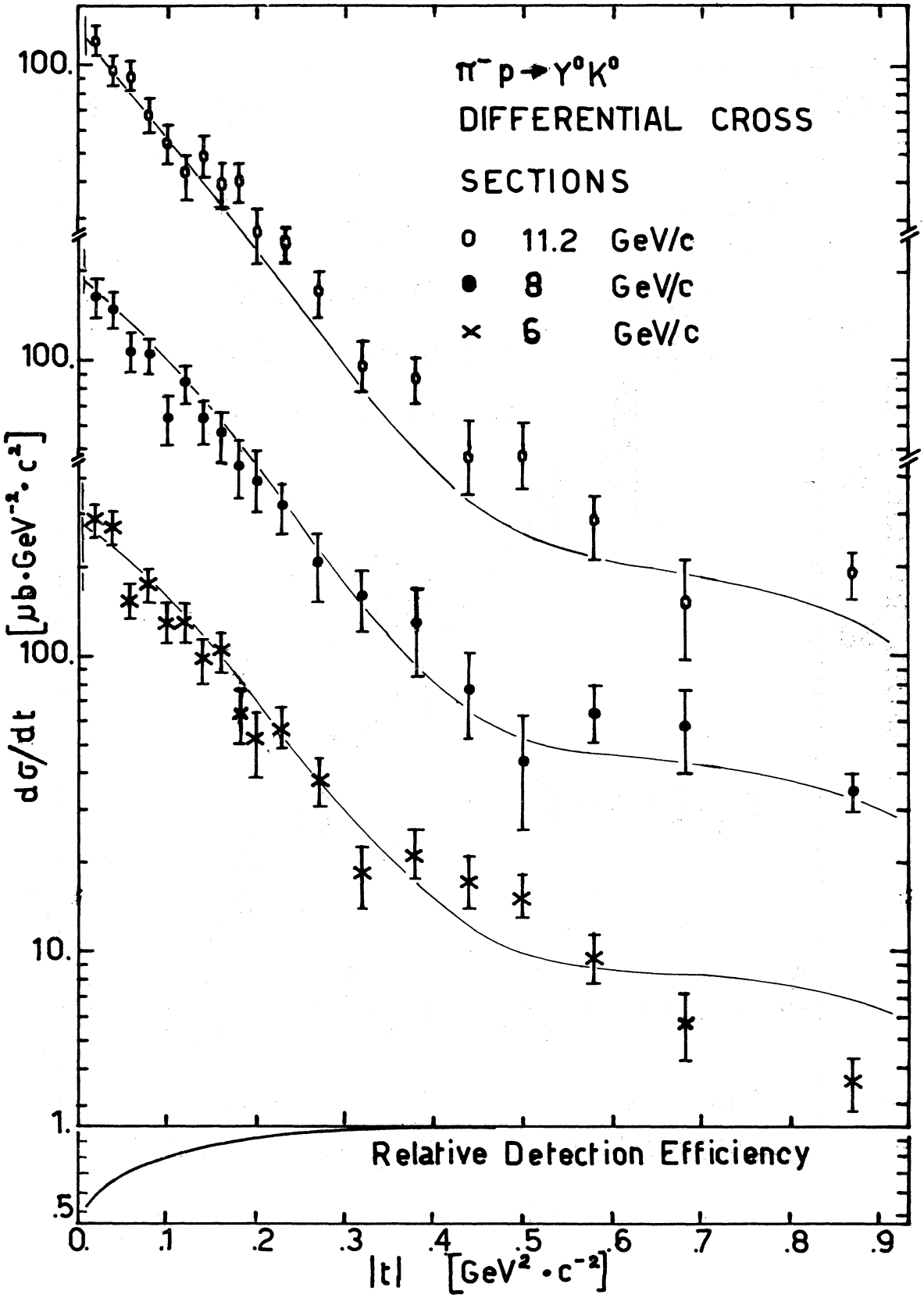
$\pi^- p \to Y^0 K^0$
DIFFERENTIAL CROSS SECTIONS
o 11.2 GeV/c
● 8 GeV/c
× 6 GeV/c
100.
100.
100.
10.
1.
.5
dσ/dt [μb·GeV⁻²·c²]
Relative Detection Efficiency
0.
.1
.2
.3
.4
.5
.6
.7
.8
.9
|t| [GeV²·c⁻²]

FIG. 5

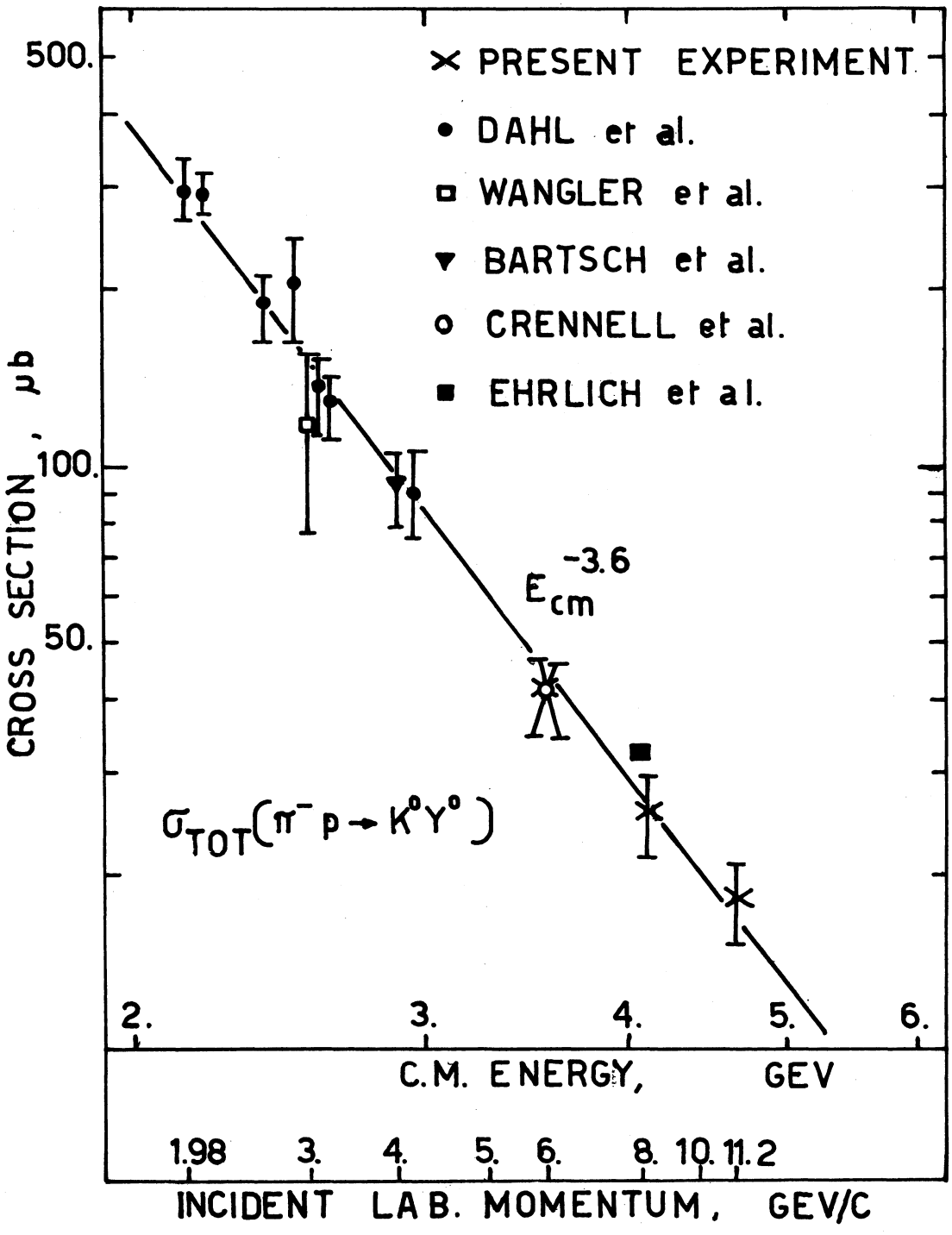
500.
100.
50.
CROSS SECTION, μb
× PRESENT EXPERIMENT
• DAHL et al.
□ WANGLER et al.
▼ BARTSCH et al.
○ CRENNELL et al.
■ EHRLICH et al.
$E_{cm}^{-3.6}$
$\sigma_{TOT}(\pi^- p \to K^0 Y^0)$
2.
3.
4.
5.
6.
C.M. ENERGY, GEV
1.98
3.
4.
5.
6.
8.
10.
11.2
INCIDENT LAB. MOMENTUM, GEV/C

FIG. 6

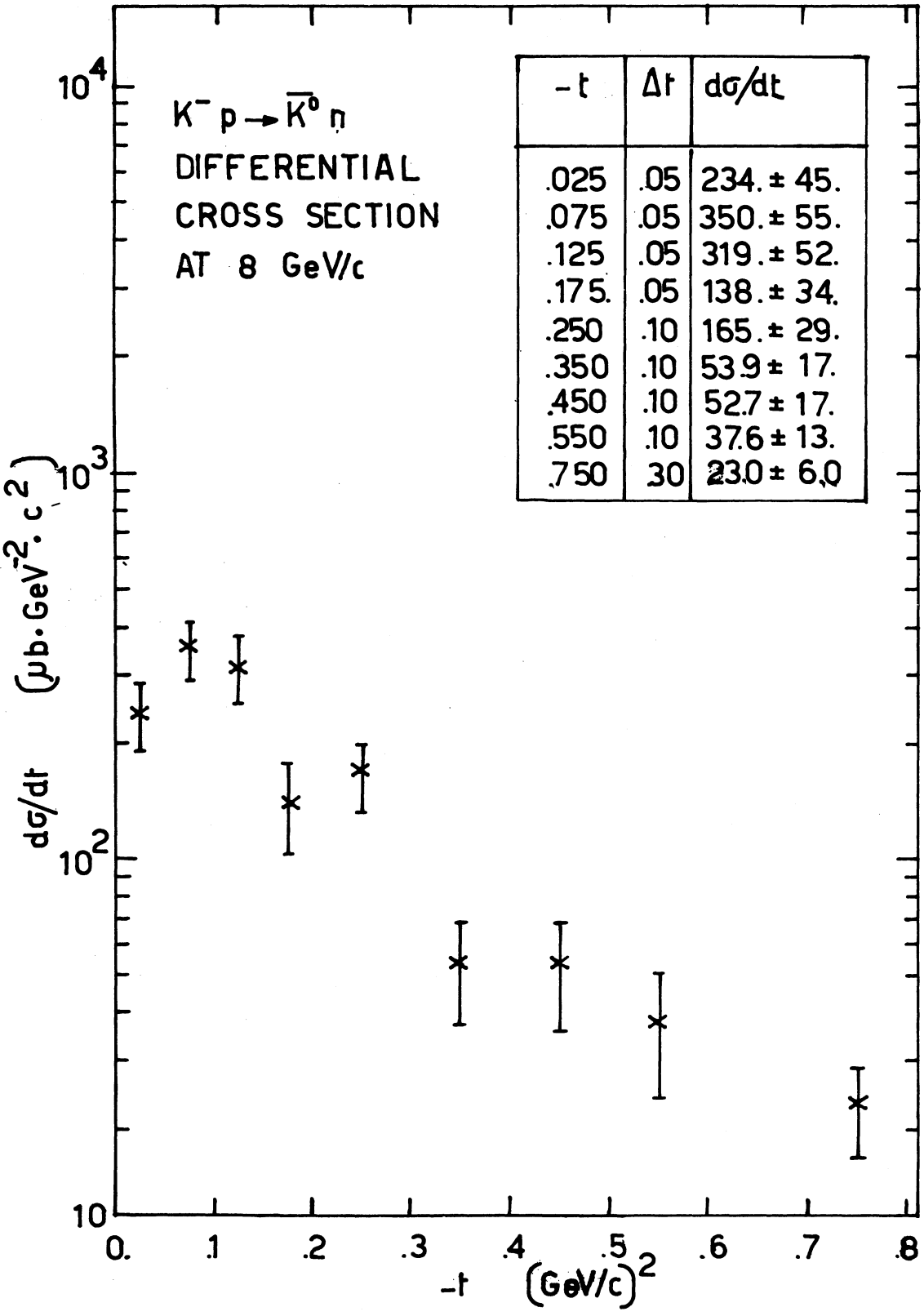


| $-t$ | $\Delta t$ | $d\sigma/dt$ |
|---|---|---|
| .025 | .05 | 234. ± 45. |
| .075 | .05 | 350. ± 55. |
| .125 | .05 | 319. ± 52. |
| .175. | .05 | 138. ± 34. |
| .250 | .10 | 165. ± 29. |
| .350 | .10 | 53.9 ± 17. |
| .450 | .10 | 52.7 ± 17. |
| .550 | .10 | 37.6 ± 13. |
| .750 | .30 | 23.0 ± 6.0 |

FIG. 7